Radiotherapy and Oncology 100 (2011) 380–385

Contents lists available at SciVerse ScienceDirect

Radiotherapy and Oncology

journal homepage: www.thegreenjournal.com

Cone beam CT

4D-CBCT reconstruction using MV portal imaging during volumetric modulated arc therapy

Satoshi Kida, Naoya Saotome, Yoshitaka Masutani, Hideomi Yamashita, Kuni Ohtomo, Keiichi Nakagawa, Akira Sakumi, Akihiro Haga*

Department of Radiology, University of Tokyo Hospital, Japan

ARTICLE INFO

Article history:
Received 23 July 2011
Received in revised form 29 August 2011
Accepted 30 August 2011
Available online 29 September 2011

Keywords:
CBCT
4D-CT
Respiratory motion
Portal imaging
VMAT

ABSTRACT

Background: Recording target motion during treatment is important for verifying the irradiated region. Recently, cone-beam computed tomography (CBCT) reconstruction from portal images acquired during volumetric modulated arc therapy (VMAT), known as VMAT-CBCT, has been investigated. In this study, we developed a four-dimensional (4D) version of the VMAT-CBCT.

Materials and methods: The MV portal images were sequentially acquired from an electronic portal imaging device. The flex, background, monitor unit, field size, and multi-leaf collimator masking corrections were considered during image reconstruction. A 4D VMAT-CBCT requires a respiratory signal during image acquisition. An image-based phase recognition (IBPR) method was performed using normalised cross correlation to extract a respiratory signal from the series of portal images.

Results: Our original IBPR method enabled us to reconstruct 4D VMAT-CBCT with no external devices. We confirmed that 4D VMAT-CBCT was feasible for two patients and in good agreement with in-treatment 4D kV-CBCT.

Conclusion: The visibility of the anatomy in 4D VMAT-CBCT reconstruction for lung cancer patients has the potential of using 4D VMAT-CBCT as a tool for verifying relative positions of tumour for each respiratory phase.

Radiotherapy is complex and verification of treatment is crucial. Although portal images acquired during treatment with an electronic portal imaging device (EPID) have been used as a planar image guidance tool and for geometrical quality assurance, the recent development of EPID dosimetry has provided in vivo dosimetry verification [1–3]. A Linac-mounted kV-CBCT is a powerful tool for verifying anatomical positions [4,5]. Accompanying rotational treatment such as volumetric modulated arc therapy (VMAT), in-treatment kV-CBCT images that reflect the patient's treatment position can be acquired just after the treatment [6–8]. The four-dimensional (4D) version known as 'in-treatment 4D kV-CBCT' verifies the positions of targets, such as lung tumours, with respiratory motion [9]. Acquiring CBCT images during treatment requires an orthogonal imager and a Linac-mounted kV source, and the isocentre displacement of the kV beam from the treatment beam must be carefully considered. More importantly, in-treatment kV-CBCT could expose the patient to additional radiation.

Recently, CBCT reconstruction with portal images during VMAT or VMAT-CBCT has been investigated [10]. The advantages of VMAT-CBCT are (1) no additional radiation exposure and (2) reduced hardware requirements, making the VMAT-CBCT a promising tool for verification of irradiated areas and/or in vivo dosimetry.

The 4D version of CBCT still presents a problem in acquiring respiratory signals for portal images. Generally, there are two methods to synchronously measure a respiratory signal with image acquisition. One method uses an image-based phase recognition (IBPR) technique [11–13]. The other uses an external respiratory monitoring system (e.g. AZ-733V by Anzai Medical Cooperation and real-time position management by Varian Medical System) [14]. This study tested the IBPR technique. For kV-CBCT, a technique of tracking small regions through the time series of projection images based on a maximum normalised cross correlation (NCC) was developed [9]. With this technique, parameters such as the size of the area were adjusted for application to portal images.

This paper reports on the feasibility of using 4D VMAT-CBCT as a treatment verification tool in two lung cancer patients receiving VMAT. Validity was assessed by comparing the tumour positions between 4D VMAT-CBCT images and in-treatment 4D kV-CBCT images simultaneously acquired during VMAT delivery. The 4D VMAT-CBCT images were also evaluated with phantom testing.

* Corresponding author. Address: Department of Radiology, The University of Tokyo Hospital, 7-3-1 Hongo, Bunkyo-ku, Tokyo 113-8655, Japan.
E-mail address: haga-haga@umin.ac.jp (A. Haga).

0167-8140/$ - see front matter © 2011 Elsevier Ireland Ltd. All rights reserved.
doi:10.1016/j.radonc.2011.08.047

Methods and materials

Outlook of the 4D VMAT-CBCT reconstruction process

4D VMAT-CBCT reconstruction is performed as follows: VMAT for lung cancer was delivered with an Elekta Synergy accelerator operating at 6 MV. During beam delivery, portal images were sequentially collected by EPID with an interval of 0.46 s using Elekta iViewGT software. The portal image consists of 1024 × 1024 pixels with a size of 0.25 mm at the isocentre. At maximum, 256 projection images per reconstruction were obtained. In order to connect the portal images with the corresponding gantry angles, we employed a log file via the Elekta software protocol, iCom, which records the gantry angle information during treatment. This was followed by matching the multi-leaf collimator (MLC) shapes derived from the portal images with those from iCom.

The acquired portal images can include the shift due to the geometric non-idealities in the rotation of the gantry system. The geometric non-idealities were measured in advance for gantry angle intervals of 5 degrees by analysing 10 cm × 10 cm radiation fields; this correction (flex correction) was performed for each portal image. The response of EPID was also regularised by considering the background (BG), linearity of monitor unit (MU), and field size (output factor) effects. MLC masking correction was performed according to Poludniowski et al. [10]. The MLC masking correction extrapolates the data truncated by the MLC field shape to mitigate artifacts otherwise induced by the filter operation of the CBCT reconstruction algorithm. A value in the masked region can be adjusted arbitrarily if we are interested only in visual images, not quantitative densities, within the patient. We defined the masking factor as a ratio of the maximum pixel value. In this study, we applied masking factors of 0.56 and 0.76 for patients 1 and 2, respectively.

Reconstruction of 4D VMAT CT requires a respiratory phase in the system. In this study, portal-image based phase recognition (P-IBPR) was employed using NCC (see below). The periodic selection of portal images of only one specific respiratory phase enables image reconstruction for that phase. Projection images were classified into 4 phases and the reconstructions were performed with a filtered back-projection (FBP) algorithm. The sequential process was performed off-line.

Portal-image based phase recognition (P-IBPR)

The method proposed here employs NCC with limited areas between adjacent portal images. Several rectangular areas ($w \times h = 5 \times 100$ pixels) are placed sequentially within exposed fields on each frame of the portal images to account for tumour motion. While a rectangular area in the current frame is fixed, an area on the next frame is moved so that the NCC value of the two areas is maximised. Movement is limited to the cranio-caudal axis. The position of the rectangular area was set to the initial position with respect to each portal image (see Fig. 1). By performing

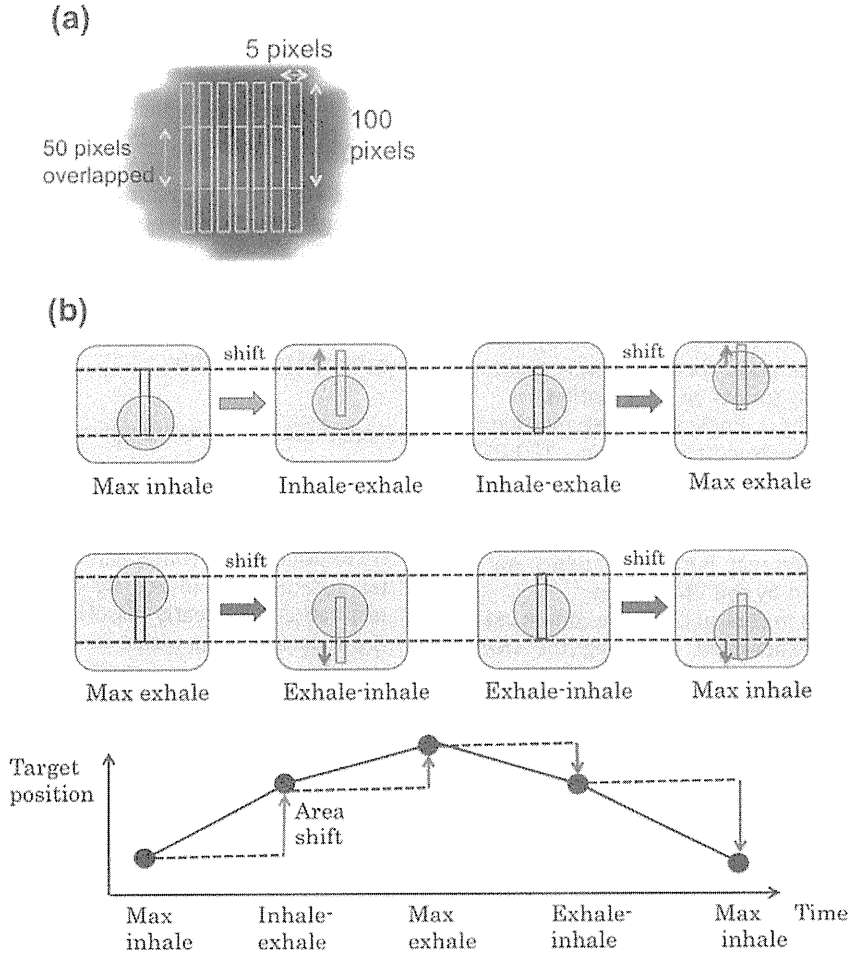

Fig. 1. (a) The distribution of several rectangular areas ($w \times h = 5 \times 100$ pixels) to cover tumour motion within exposed fields on each portal image. They are partially overlapped. (b) Schematic explanation of P-IBPR using NCC. The positions of the rectangular areas are shifted only along the cranio-caudal axis on the next portal image to find the maximum value of NCC with the calculation area on the previous portal image. The position of the rectangular area was set to the initial position with respect to each portal image. For the above example, the black rectangles indicate initial position and red rectangles indicate the position that gives the maximum NCC value with the corresponding black rectangles.

this procedure repeatedly for all portal images, a respiration signal can be obtained by displacement in the cranio-caudal direction. The signals were averaged among the calculation areas. Finally, low periodic components more than 5 s and high periodic components less than 1 s were removed in the frequency domain by using the band pass filter. The phase distributions were phase 0% (max inhale), phase 25% (inhale–exhale), phase 50% (max exhale), and phase 75% (exhale–inhale).

The efficiency of P-IBPR was determined by comparing the breathing pattern acquired by P-IBPR with those measured by visual tracking of the tumour on portal images. Here, the breathing cycle period was defined as the interval between adjacent max-expiration phases. In the visual tracking, a slight shaking can be recognised as a peak of expiration. Therefore, respirations with amplitudes less than 1 mm were neglected in the detection of max exhale.

Treatment planning for VMAT

One potential problem when inverse planning for lung cancer treatment is that the optimisation of beam fluences only takes into account a single three-dimensional volumetric data set. For this, the actual VMAT that continuously delivers the dose in all respiratory phases, may yield a dose distribution that differs from the plan. In order to compensate for this fact, the target volume can be extended to encompass the range of target motion by using 4D-CT scan, and field shapes can be defined as the target surroundings. Alternatively, the inverse plan that constrains MLC motion in VMAT forms field shapes that do not hide the target in lung cancer treatment. In this case, the beam intensity is mainly modulated by changing gantry speed and dose rate.

In this study, the planning target volume (PTV) for the lung tumour was created with a 5-mm margin of internal target volume generated from 20 4D-CT sets by using a 320-slice volumetric CT scanner (TOSHIBA, Japan). The patients received a D95 prescription of 50 Gy for PTV in 4 fractions. The single-arc VMAT with 6 MV was created by SmartArc in the Pinnacle v9.0 treatment planning system (Philips, USA). The constraint on MLC motion of 0.1 cm/degree was applied in the VMAT inverse plan so that MLC had little chance to hide the PTV. Such a constraint on MLC motion may significantly affect the quality of a treatment plan. Therefore, these plans were compared to those without constraints on MLC motion.

Treatment was performed by a single clockwise rotation (360 degrees). The arc used for reconstruction was from −180 to −19 degrees (patient 1) and from −180 to −40 degrees (patient 2). The angle range to allow portal imaging was limited by the Elekta iView software such that the maximum number of sequential acquisitions was 256. The difference between patients was due to the gantry speed determined by the VMAT plan.

Before applying the method to clinical cases, we conducted a 4D VMAT-CBCT reconstruction experiment by using the QUASAR respiratory motion phantom (Modus Medical Devices Inc.). The mechanical amplitude and cycle in the phantom were set at 10 mm and 3 s, respectively. The VMAT plan for patient 1 was delivered.

Result

VMAT plan with the MLC constraint

The dose-volume histograms (DVHs) for patients 1 and 2 are shown in Fig. 2a and b, respectively. The solid curves denote the DVHs with an MLC constraint of 0.1 cm/degree, while the dashed curves denote DVHs without MLC constraints. The dose homogeneity of the plan without MLC constraint was better than the plan with MLC constraint for both patients. Dose conformity was

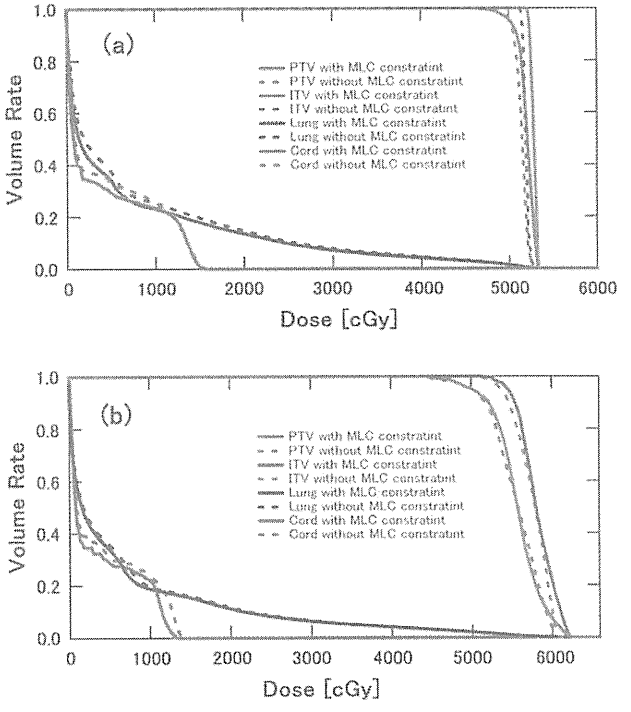

Fig. 2. DVH with and without MLC constraints for (a) patient 1 and (b) patient 2, All plans were prescribed as D95 of PTV equal to 50 Gy. The solid curves denote the DVHs with MLC constraint of 0.1 cm/degree, while the dashed curves denote those without MLC constraint.

comparable. On the other hand, the DVHs for organ at risk (OAR) with MLC constraint were slightly better than the DVHs without MLC constraint. This is presumably because in inverse planning, the constraint on homogeneity and conformity for PTV was stronger than the DVH constraint on OAR.

We found little difference between the plans with and without MLC constraints in the tested patients. The plans with MLC constraints were acceptable for clinical use and the MLC constraint was judged to manage the target motion without significant degradation of plan quality.

Acquisition of respiratory signal

The respiratory behaviours of two patients assessed by our P-IBPR method are shown in Fig. 3a and b. The original signal could have pseudo periodic components, such as those generated by gantry rotation. These components were removed by the band pass filter and, as seen in Fig. 3c and d, the motion due to patient respiration was clearly dissolved in all gantry angle directions. In Fig. 4, the breathing cycles were compared with those derived from the tumour motion in visual tracking. In Fig. 4a and b for patient 1, the breathing cycle was estimated by 3.7 ± 0.4 (1 SD) for both P-IBPR and visual tracking, while in Fig. 4c and d for patient 2, the breathing cycle was estimated by 2.7 ± 0.3 (1 SD) and 2.7 ± 0.4 (1 SD) for P-IBPR and visual tracking, respectively. The result in P-IBPR was concordant with the result of visual tracking. The difference of breathing cycle between P-IBPR and visual tracking was one sampling time (0.46 s) at most.

Reconstruction of 4D VMAT-CBCT in phantom

The reconstruction images of 4D VMAT-CBCT with an FBP algorithm corresponding to the points of maximum oscillation are shown in Fig. 5a and b. The standard calculation time for reconstruction with 270 × 270 × 80 voxels was about 10 s by GPU using

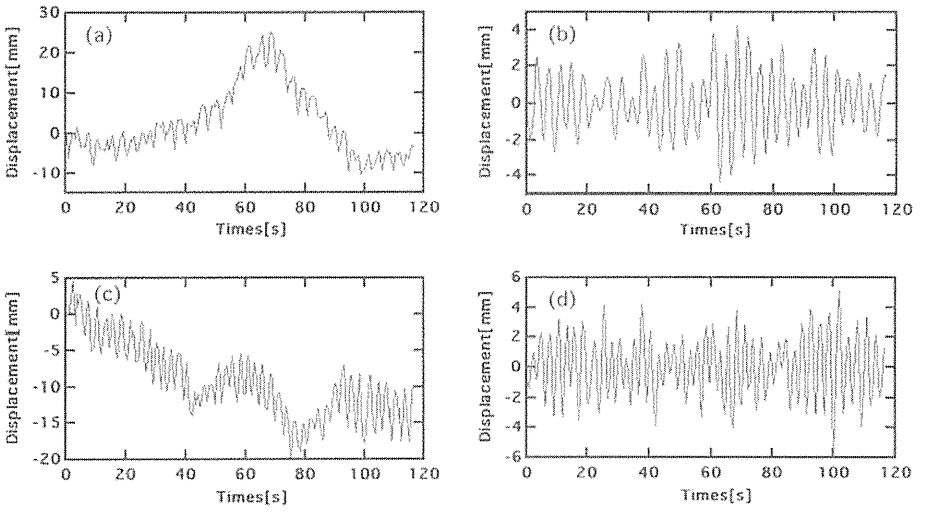

Fig. 3. Respiratory signal acquired by P-IBPR for patient 1 (a) before filtering and (b) after filtering and for patient 2 (c) before filtering and (d) after filtering.

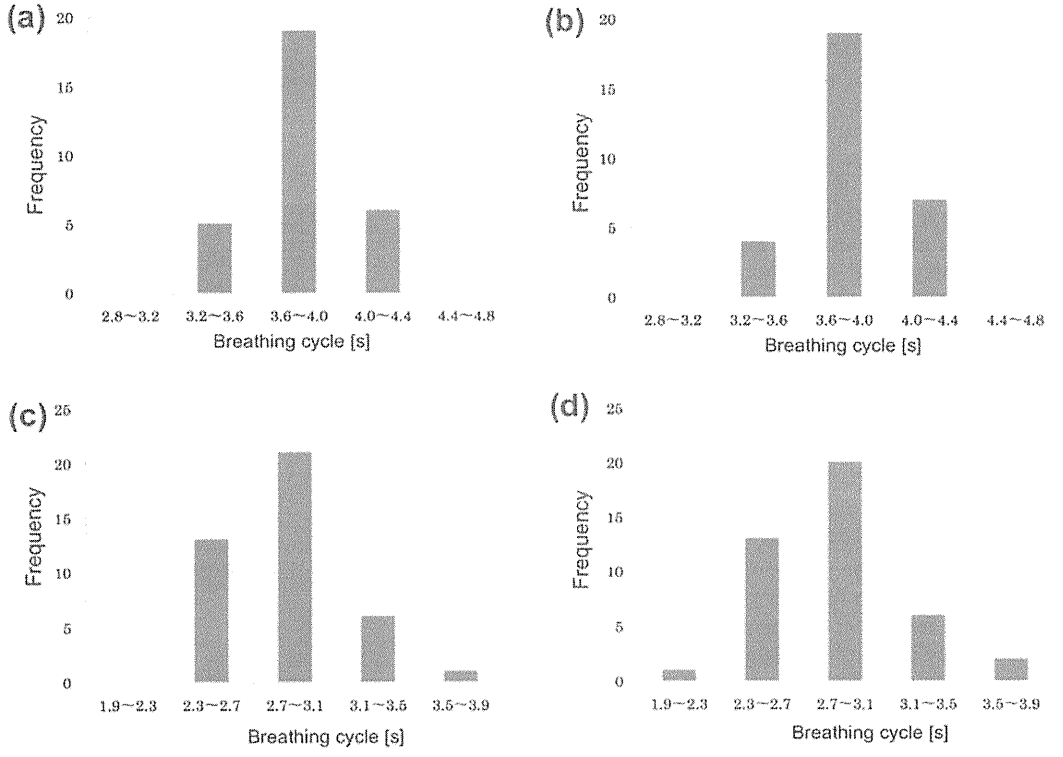

Fig. 4. Histograms of breathing cycle analysed by P-IBPR and visual tracking; (a) P-IBPR and (b) visual tracking for patient 1 and (c) P-IBPR and (d) visual tracking for patient 2.

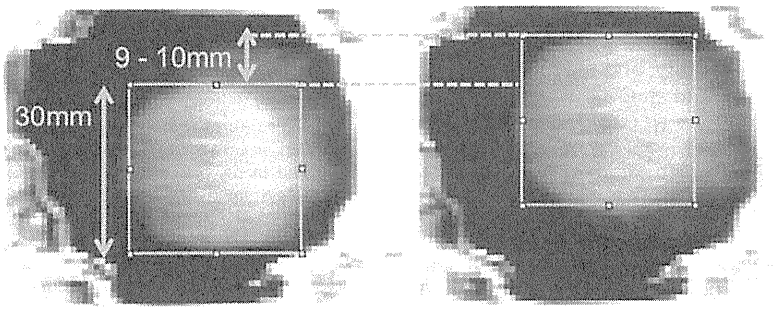

Fig. 5. Coronal images of 4D VMAT-CBCT of the QUASAR phantom in each peak. The diameter of the ball was 30 mm. The displacement was evaluated to be about 9–10 mm.

NAVIDIA Tesla C1060 4 GB. The amplitude was evaluated at about 9–10 mm from the 4D VMAT-CBCT images. This displacement is close to the mechanical set of 10 mm in the experiment. The inhomogeneous value inside the insert was observed.

Reconstruction of 4D VMAT-CBCT in 2 patients

With the respiratory signals acquired by P-IBPR, the portal images were classified into 4 phase bins. Then, VMAT-CBCT reconstruction was performed. For comparison, kV projection images were simultaneously acquired during VMAT, and 4D kV-CBCT was reconstructed. Fig. 6a and b illustrate the coronal and sagittal slices of VMAT-CBCT and kV-CBCT for 3D and the respiratory phases (max exhale, exhale inhale, max inhale, and inhale exhale) of patients 1 and 2.

The total number of portal images acquired during VMAT was 254 for both patients. Those images were almost equally classified into each phase bin. The gantry angle increment per projection for 4D reconstruction is dependent not only on the gantry speed but also on the respiratory cycle of the patient. These values for patients 1 and 2 were estimated as 5.4 ± 0.8 (1SD) and 3.9 ± 0.5 (1SD) degrees, respectively. Admittedly, there were large projection gaps that degraded image quality. In addition, this "effective" gantry angle increment included the error caused by the long acquisition interval of portal images, which was limited to 0.46 s per projection.

The centre of mass (COM) positions of the tumour during treatment were estimated from a contour of the tumour in respective max-exhale volume images in the Pinnacle treatment planning system and by shifting these contours in the other images. The shifts from the max exhale are denoted in Fig. 6. The results of 4D MV-CBCT were remarkably close to those of 4D kV-CBCT. The amplitudes of tumour motion during treatment for patients 1 and 2 were estimated to be about (1, 2, 5) and (2, 4, 5) mm, respectively. On the other hand, it was difficult to estimate tumour size due to diminished image quality and artifacts.

Discussion

It should be noted that an exact and unique cone-beam reconstruction from portal images acquired in a VMAT delivery is impossible in principle [10]. That is, the VMAT-CBCT including our method is based on the assumption that there are few structures outside the radiation field. The effect of passing through objects outside the reconstructed region is naively considered by masking correction. However, as seen in Figs. 5 and 6 4D VMAT-CBCT showed the tumour position to be similar when predicted mechanically by the phantom and by the 4D kV-CBCT. We emphasise that we are interested in the visualisation of tumour motion for verification of actual treatment. From this viewpoint, we are satisfied that the amplitude can be evaluated from the 4D VMAT-CBCT images. Our method is, therefore, feasible for verifying tumour motion through the course of treatment. On the other hand, it should be noted that inconsistencies, such as the lack of projection data provided the degradation of image quality, and may lead to incorrect recognition for the tumour size and shape.

We employed the IBPR method using NCC to derive respiratory signals from portal images. Our experiments demonstrated that NCC can work well for frame-by-frame changes in irradiation intensity. Respiratory signals were readily obtained because the MLC speed was constrained by treatment planning optimisation. This constraint yielded field shapes similar to those created in conformal treatment. The fact that the tumour was located in the middle of the lung may explain why the MLC did not need to move drastically. Thus, a target was detected within a field through

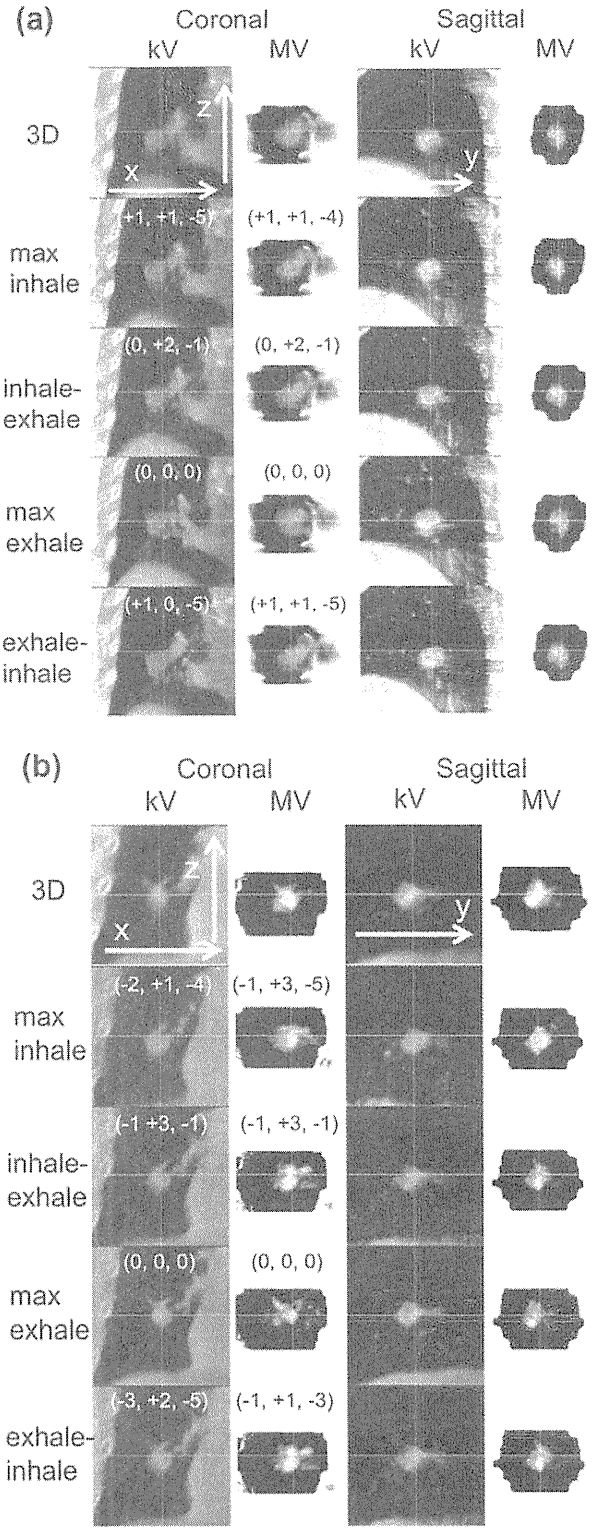

Fig. 6. Coronal and sagittal images at the isocentre plane of in-treatment kV 3D- and 4D-CBCT and 3D- and 4D-VMAT CT for (a) patient 1 and (b) patient 2. The coordinates inside the images represent the COM of tumour shift from max exhale with units in mm for each modality. The COMs were estimated from a contour delineated in respective max-exhale volume images on the Pinnacle treatment planning system and by shifting the contour in the other images.

almost all angles. On the other hand, the MLC constraint in the inverse plan may hinder clinical utility due to degradation of plan quality. In our clinical cases, this degradation was small and we judged that suppressing the MLC motion was beneficial for the

moving target. Of course, we cannot generalise our results, as this study was limited to 2 patients.

One of the advantages of IBPR is that no extra devices are required. It also provides direct tracking of tumour motion in contrast to methods that require external devices. In addition, correlations in the motion of inner structures and the body surface are not always measurable by external devices [15]. This is a critical problem for 4D-CT reconstruction.

In addition to our NCC method, several IBPR techniques such as the Amsterdam shroud method [11,12] and Kavanagh's method [13] have been proposed to acquire respiratory signals for kV projection images. The former projects 2D images onto the cranio-caudal axis to obtain a 1D signal for each image, while the latter utilises changes in the pixel value summation within each projection image. Both methods are based on pixel value projection and are easily affected by MLC motion, which yields drastic changes in pixel values within the projection images even if the MLC motion is as small as it was in our cases. Therefore, these methods would have difficulty with portal images.

Current issues or limitations of VMAT-CBCT reconstruction include the influence of intensity distribution and the shape yielded by MLC on the projection images. We performed a homogeneous correction of the total intensity within a field depending on the size and monitor unit. However, the change in field size yields an inhomogeneous intensity within the field, a matter that must be addressed in future studies. In addition, due to limitations of the Elekta iView software, the maximum number of portal imaging sequential acquisitions is only 256, so the acquisition of images may be insufficient for longer treatments. For stable P-IBPR, a sampling interval should be short enough to acquire a respiratory signal. Therefore, in this study, the shortest sampling rate of the Elekta iView software was employed, and the portal imaging was performed during less than half of a gantry rotation.

The inhomogeneous value inside the insert of the phantom as seen in Fig. 5 was also partly caused by this limitation. Optimised operation for the acquisition of portal images should be allowed in the system. Alternatively, a reconstruction algorithm can be developed as represented by digital tomosynthesis [16,17] and by compressed sensing [18] for a limited acquisition angle. The removal of such problems will enable quantitative derivation of 4D VMAT-CBCT.

In conclusion, a 4D VMAT-CBCT reconstruction technique was developed by using P-IBPR with the NCC method, which enabled us to obtain in-treatment volume images in 4 phases. The visibility of the anatomy in 4D VMAT-CBCT reconstruction for lung cancer patients makes this a promising tool for verifying relative tumour positions for each respiratory phase.

Acknowledgements

This work was partially supported by JSPS KAKENHI 22791176. S.K. and A.H. wish to thank Dr. Grant Jackson (Elekta K.K.) for his advice regarding the use of iCom to acquire log data during treatment. K.N. received research funding from Elekta K.K.

References

[1] van Elmpt W, McDermott L, Nijsten S, et al. A literature review of electronic portal imaging for radiotherapy dosimetry. Radiother Oncol 2008;88:289–309.
[2] Nijsten SM, Mijnheer BJ, Dekker AL, et al. Routine individualized patient dosimetry using electronic portal imaging devices. Radiother Oncol 2007;83:65–75.
[3] McDermott LN, Wendling M, Sonke JJ, et al. Replacing pretreatment verification with in vivo EPID dosimetry for prostate IMRT. Int J Radiat Oncol Biol Phys 2007;67:1568–77.
[4] Murphy MJ, Balter J, Balter S, et al. The management of imaging dose during image-guided radiotherapy: report of the AAPM Task Group 75. Med Phys 2007;34:4041–6063.
[5] Balter J, Benedict S, Bissonnette JP, et al. The role of in-room kV X-ray imaging for patient setup and target localization, AAPM Report No. 104. American Association of Physics in Medicine, 2009.
[6] Nakagawa K, Yamashita H, Shiraishi K, et al. Verification of in-treatment tumour position using kilovoltage cone-beam computed tomography: a preliminary study. Int J Radiat Oncol Biol Phys 2007;69:970–3.
[7] Nakagawa K, Haga A, Shiraishi K, et al. First clinical cone-beam CT imaging during volumetric modulated arc therapy. Radiother Oncol 2009;90:422–3.
[8] Ling C, Zhang P, Etmektzoglou T, et al. Acquisition of MV-scatter-free kilovoltage CBCT images during RapidArc™ or VMAT. Radiother Oncol 2011;100:145–9.
[9] Nakagawa K, Kida S, Haga A, et al. Cone beam computed tomography data acquisition during VMAT delivery with subsequent respiratory phase sorting based on projection image cross-correlation. J Radiat Res (Tokyo) 2011;52:112–3.
[10] Poludniowski G, Thomas MDR, Evans PM, et al. CT reconstruction from portal images acquired during volumetric-modulated arc therapy. Phys Med Biol 2011;55:5635–51.
[11] Sonke JJ, Zijp L, Remeijer P, van Herk M. Respiratory correlated cone beam CT. Med Phys 2005;32:1176–86.
[12] Zijp L, Sonke J, van Herk M. Extraction of the respiratory signal from sequential thorax cone-beam X-ray images. Jeong Publishing (Seoul) 2004:507–9.
[13] Kavanagh A, Evans PM, Hansen VN, et al. Obtaining breathing patterns from any sequential thoracic X-ray image set. Phys Med Biol 2009;54:4879–88.
[14] Otani Y, Fukuda I, Tsukamoto N, et al. A comparison of the respiratory signals acquired by different respiratory monitoring systems used in respiratory gated radiotherapy. Med Phys 2010;37:6178–86.
[15] Korreman SS, Juhler-Nottrup T, Boyer AL. Respiratory gated beam delivery cannot facilitate margin reduction, unless combined with respiratory correlated image guidance. Radiother Oncol 2008;86:61–8.
[16] Maurer J, Godfrey D, Wang Z, et al. On-board four-dimensional digital tomosynthesis: first experimental results. Med Phys 2008;35:3574–83.
[17] Maurer J, Pan T, Yin FF. Slow gantry rotation acquisition technique for on-board four-dimensional digital tomosynthesis. Med Phys 2010;37:921–33.
[18] Choi K, Wang J, Zhu L, et al. Compressed sensing based cone-beam computed tomography reconstruction with a first-order method. Med Phys 2010;37:5113–25.

Technical Note: Extension of van Herk's treatment margin model for anisotropic systematic positioning errors in Cartesian coordinate system[a)]

Kiyoshi Yoda[b)]
Elekta KK, 3-9-1 Shibaura, Minato-ku, Tokyo 108-0023, Japan

Keiichi Nakagawa
Department of Radiology, University of Tokyo Hospital 7-3-1 Hongo, Bunkyo-ku, Tokyo 113-8655, Japan

(Received 11 April 2011; revised 6 May 2011; accepted for publication 10 May 2011; published 16 June 2011)

Purpose: A coefficient of a treatment margin model for anisotropic systematic positioning errors has been calculated in Cartesian coordinate system based on van Herk's analytical formulation.
Methods: Three-dimensional (3D) patient population distribution was formulated in Cartesian coordinate system to model anisotropic systematic positioning errors. Analytical 3D integration with anisotropic standard deviations Σ's and the following Newton's method yielded the coefficient of van Herk's systematic positioning error model in Cartesian coordinate system.
Results: The treatment margins for the anisotropic systematic errors in Cartesian coordinate system were 2.1 Σ for 90% patient population coverage and 2.4 Σ for 95% patient population coverage.
Conclusions: It was found that the treatment margins for anisotropic systematic positioning errors in Cartesian coordinate system were smaller than those for the isotropic model in spherical coordinate system for a given patient population coverage probability. © *2011 American Association of Physicists in Medicine.* [DOI: 10.1118/1.3596531]

Key words: treatment margin, Cartesian coordinate system, systematic positioning errors

Marcel van Herk *et al.* proposed an analytical treatment margin model that considered both systematic positioning errors among all the patients in a facility and random positioning errors among all the treatment fractions for each patient.[1,2] The coefficients of the model parameters were numerically calculated under a spherically symmetric condition thereby leading to an isotropic margin perpendicular to a spherical tumor surface. However, recent high precision treatment is performed under Cartesian coordinate system with a 3 or 6 degrees-of-freedom couch, and the systematic positioning errors may be anisotropic. Although the original article mentioned an extension to anisotropic modeling,[1] detailed results have not been published.

In this article, three-dimensional (3D) Gaussian patient population is formulated in Cartesian coordinate system to model anisotropic systematic errors for patient positioning. Analytical integration with anisotropic standard deviations and the following Newton's method are performed to derive the coefficient of van Herk's systematic positioning error model in Cartesian coordinate system.

The 3D Gaussian patient population model is given by

$$G(x,\Sigma_x^2)G(y,\Sigma_y^2)G(z,\Sigma_z^2), \tag{1}$$

where $G(r,\Sigma_r^2)$ denotes the probability density of one-dimensional Gaussian distribution with a standard deviation of Σ_r, where r is x, y, or z. For example, $G(x,\Sigma_x^2)$ is given by

$$G(x,\Sigma_x^2) = \frac{e^{-\frac{x^2}{2\Sigma_x^2}}}{\sqrt{2\pi}\Sigma_x}. \tag{2}$$

The coverage probability of the patient population in the systematic positioning error ranges of $-c\ \Sigma_x < x < c\ \Sigma_x$, $-c\ \Sigma_y < y < c\ \Sigma_y$, and $-c\ \Sigma_z < z < c\ \Sigma_z$ is given by 3D integration of (1) leading to

$$\mathrm{erf}\left(\frac{c}{\sqrt{2}}\right)^3 \tag{3}$$

where c is an arbitrary positive constant, and erf is the error function. The analytical integration was performed by a computer code, Mathematica,[3] as shown in Fig. 1.

The expression (3) is a trivial form because it is the third power of the one-dimensional result shown in van Herk's paper,[1] however, to the author's knowledge it has not been calculated nor compared to the original van Herk's coefficient in spherical coordinate system. To solve the nonlinear equation, Newton's method was employed and the results are shown in Table I. Again, the numerical root finding was performed by Mathematica,[3] which is also shown in Fig. 1. It was found that the treatment margins for anisotropic systematic positioning errors in Cartesian coordinate system were smaller than those for the isotropic model in spherical coordinate system for a given patient population coverage probability.

In conclusion, van Herk's treatment margin model for systematic errors was reformulated by calculating the coefficient of the anisotropic systematic error model in Cartesian coordinate system. The resulting coefficient was smaller than that for the spherically symmetric model.

Further modification would be possible by integrating (1) with varied integration ranges in 3D directions. Meanwhile,

```
gaussian3Danisotropic =
  Function[{x, y, z},
         Exp[-x^2 / (2 sigmax^2)] / sigmax / Sqrt[2 Pi] *
         Exp[-y^2 / (2 sigmay^2)] / sigmay / Sqrt[2 Pi] *
         Exp[-z^2 / (2 sigmaz^2)] / sigmaz / Sqrt[2 Pi]
  ]
```

$$\text{Function}\left[\{x, y, z\}, \frac{e^{-\frac{x^2}{2\,\text{sigmax}^2}}\, e^{-\frac{y^2}{2\,\text{sigmay}^2}}\, e^{-\frac{z^2}{2\,\text{sigmaz}^2}}}{(\text{sigmax}\sqrt{2\pi})\,(\text{sigmay}\sqrt{2\pi})\,(\text{sigmaz}\sqrt{2\pi})}\right]$$

```
Integrate[
  gaussian3Danisotropic[x, y, z],
     {x, -Infinity, Infinity}, {y, -Infinity, Infinity}, {z, -Infinity, Infinity},
       Assumptions → {sigmax > 0, sigmay > 0, sigmaz > 0}
]
```

```
1
```

```
Integrate[
  gaussian3Danisotropic[x, y, z],
     {x, -c sigmax, c sigmax}, {y, -c sigmay, c sigmay}, {z, -c sigmaz, c sigmaz}
]
```

$$\text{Erf}\left[\frac{c}{\sqrt{2}}\right]^3$$

$$\text{FindRoot}\left[\text{erf}\left(\frac{c}{\sqrt{2}}\right)^3 = 0.8, \{c, 1.\}\right]$$

```
{c → 1.80113}
```

$$\text{FindRoot}\left[\text{erf}\left(\frac{c}{\sqrt{2}}\right)^3 = 0.85, \{c, 1.\}\right]$$

```
{c → 1.93711}
```

$$\text{FindRoot}\left[\text{erf}\left(\frac{c}{\sqrt{2}}\right)^3 = 0.9, \{c, 1.\}\right]$$

```
{c → 2.11405}
```

$$\text{FindRoot}\left[\text{erf}\left(\frac{c}{\sqrt{2}}\right)^3 = 0.95, \{c, 1.\}\right]$$

```
{c → 2.38774}
```

$$\text{FindRoot}\left[\text{erf}\left(\frac{c}{\sqrt{2}}\right)^3 = 0.99, \{c, 1.\}\right]$$

```
{c → 2.93416}
```

FIG. 1. A computer code for calculating the coefficient of van Herk's treatment margin model for anisotropic systematic positioning errors in Cartesian coordinate system. Each bold part is a command followed by each calculated result.

TABLE I. Treatment margins, $\alpha\ \Sigma$, for systematic positioning errors as a function of patient population coverage probability.

Patient population coverage (%)	Cartesian 3D model (Σ)	Spherical 3D model (Σ)
80	1.80	2.16
85	1.94	2.31
90	2.11	2.50
95	2.39	2.79
99	2.93	3.36

the present author believes that the most important point to keep in mind is that the present margin model excludes delineation errors in a clinical target volume.[1,2,4]

[a]Dr Nakagawa receives research funding from Elekta.
[b]Electronic mail: Kiyoshi.Yoda@elekta.com

[1]M. van Herk, P. Remeijer, C. Rasch, and J. V. Lebesque, "The probability of correct target dosage: Dose-population histograms for deriving treatment margins in radiotherapy," Int. J. Radiation Oncology Biol. Phys. **47**, 1121–1135 (2000).
[2]M. van Herk, "Errors and margins in radiotherapy," Semin. Radiat. Oncol. **14**, 52–64 (2004).
[3]S. Wolfram, *Mathematica, a System for Doing Mathematics by Computer* (Addison-Wesley, San Francisco, 1991).
[4]M. van Herk, "Will IGRT live up to its promise?," Acta Oncol. **47**, 1186–1187 (2008).

J. Radiat. Res., 52, 536–537 (2011)

First In-situ Dose Calculation Report Using In-treatment Kilovoltage Cone-beam CT and In-treatment Linac Parameters during Volumetric Modulated Arc Therapy

Akira SAKUMI[1], Akihiko HAGA[1], Satoshi KIDA[1], Naoya SAOTOME[1], Yukari OKANO[1], Kenshiro SHIRAISHI[1], Takeshi ONOE[1], Kiyoshi YODA[2], Kuni OHTOMO[1] and Keiichi NAKAGAWA[1]*

In-situ dose calculation/In-treatment cone-beam CT/Volumetric modulated arc therapy.

To the editor

Tumor registration using kilovoltage (kV) cone-beam CT (CBCT) prior to radiotherapy has been increasingly adopted for daily clinical practice. Compared to traditional two-dimensional bone registration, kV CBCT provides three-dimensional tumor registration between previously acquired planning CT and the CBCT on each treatment day. In addition, kV CBCT shows daily displacement and deformation of organs as well as regression of tumors during the course of the treatment.

As a natural next step, patient dose distribution on each treatment day has been gradually highlighted by using CBCT image data. The reported accuracy of the CBCT-based dose calculation in reference to a planning CT was within 2 to 3%.[1,2] In the meantime, we have already reported clinical kV CBCT imaging during rotational radiotherapy using a linac with a CBCT unit (Elekta, UK)[3] and volumetric modulated arc therapy (VMAT).[4] We also published a dose calculation procedure by referring to log files including actual data of multi leaf collimator (MLC) positions, jaw positions, gantry angles and MUs with an interval of every 0.25 seconds in the linac service mode.[5] Recently, Qian calculated dose distributions by combining CBCT images acquired before treatment and actual in-treatment log files stored in a Varian linac.[6] In contrast, we report the first in-situ dose calculation using in-treatment CBCT and in-treatment linac parameters during VMAT delivery, which may directly correspond to the actually absorbed dose distributions during treatment.

A treatment planning system (TPS), Pinnacle3 9.0 SmartArc (Phillips, Holland) was employed to create a single-arc VMAT plan for a prostate cancer patient. The PTV dose prescription (D_{95}) was 76 Gy in 38 fractions. The linac photon energy was 6 MV. A record and verify system, Mosaiq 1.6 (Elekta, USA), was employed with a linac control software, Desktop Pro 7.0.1 (Elekta, UK). A single-arc VMAT required approximately 120 seconds. During the VMAT delivery, a log file was recorded via iCOM interface (Elekta, UK). Subsequently, the iCom data format was converted to Pinnacle data format, thereby allowing Pinnacle to read actual MLC positions, jaw positions, gantry angles and MUs with an interval of every 0.25 seconds. During the VMAT delivery, in-treatment kV projection data were also stored and CBCT image reconstruction was performed by in-house software. By exporting these data back to the TPS, in-treatment dose distributions were obtained.

Figure 1(a) shows the resulting in-situ dose distribution calculated by the in-treatment CBCT and the in-treatment linac parameters. The innermost two contours are clinical target volume (CTV) and planning target volume (PTV) of the prostate cancer. A PTV margin of 5 mm was employed except for the rectum side with a 4 mm margin. The isodose contour lines are, from inside to outside, 107% (a tiny blue island near the PTV boundary), 95%, 90%, 80%, 70%, 60%, 50%, 30% and 10% (purple) of the prescribed dose. A CBCT value to density conversion table was created by referring to a planning CT value to density table at the corresponding pixel locations on the paired data set of the planning CT and the CBCT, in regions close to the PTV including prostate, fat, and bone anatomies. To reduce scattering effects, CBCT values were corrected, with a simple approximation, based on a reconstructed CBCT image of a water column phantom, where a non-linear correction function was determined as a function of radius from the image center. The calculated mean doses for the PTV and rectum using the planning CT and the CBCT agreed within 1.4% and 3.4%, respectively. Figure 1(b) shows in-situ isodose color map overlaid on the in-treatment CBCT image, and Fig. 1(c) shows dose distributions calculated by the planning

*Corresponding author: Phone: +81-3-5800-8786,
Fax: +81-3-5800-8786,
E-mail: k-nak@fg7.so-net.ne.jp
[1]Department of Radiology, University of Tokyo Hospital, 7-3-1 Hongo, Bunkyo-ku, Tokyo, 113-8655, Japan; [2]Elekta KK, 3-9-1 Shibaura, Minato-ku, Tokyo 108-0023, Japan.
doi:10.1269/jrr.11061

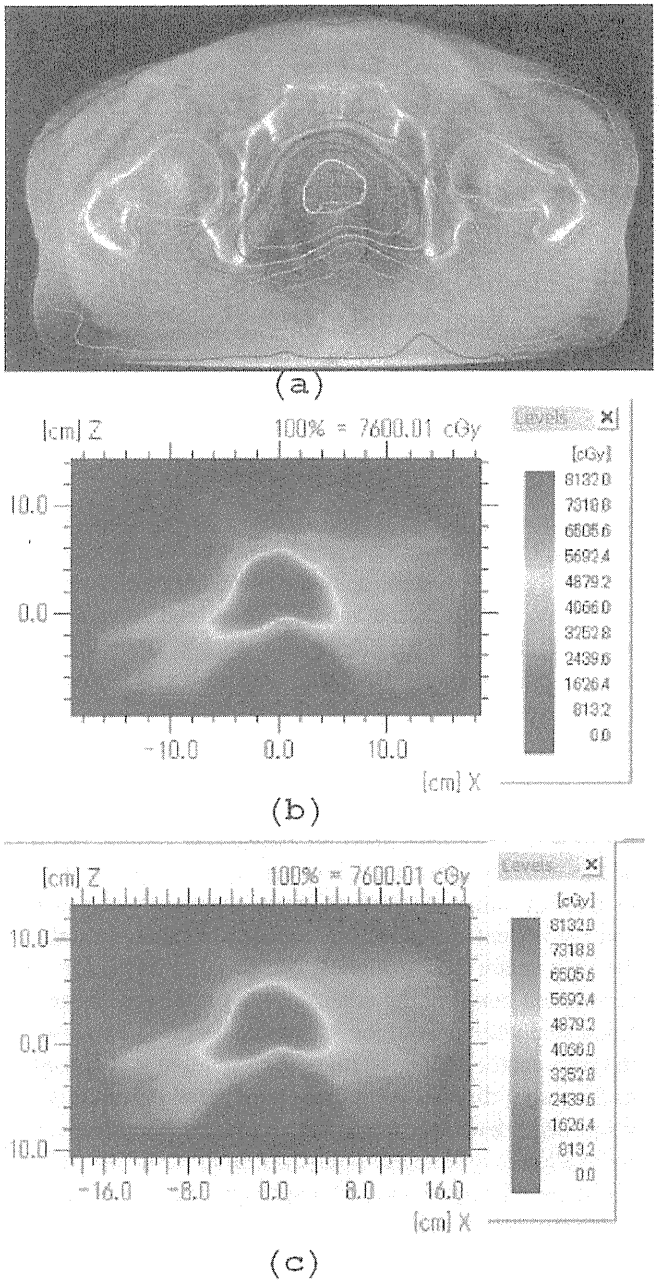

Fig. 1. In-situ dose calculation results using in-treatment cone-beam CT and in-treatment linac parameters during volumetric modulated arc therapy: (a) with isodose contours and (b) with isodose color map. An isodose color map calculated by the planning CT is shown in (c) for comparison.

CT for comparison. The pass rate of 1% dose difference between the dose distributions shown in (b) and (c) within the entire CBCT volume was 93.1%, whilst the pass rate of 2% dose difference went up to 96.5%. A reasonably good agreement was observed even if the body contour shapes were significantly different as shown at the both sides near the couch top.

In conclusion, we have shown that in-situ dose calculation during VMAT delivery is feasible by using in-treatment kV CBCT and in-treatment linac parameters. Further quantitative analysis is required to apply this technique to the next generation dose guided radiotherapy, which was originally proposed back in 2002.[7]

REFERENCES

1. Ding GX, *et al* (2007) A study on adaptive IMRT treatment planning using kV cone-beam CT. Radiother Oncol **85**: 116–125.
2. Richter A, *et al* (2008) Investigation of the usability of cone beam CT data sets for dose calculation. Radiation Oncology **3**: 42.
3. Nakagawa K, *et al* (2007) Verification of in-treatment tumor position using kilovoltage cone-beam computed tomography: preliminary study. Int J Radiat Oncol Biol Phys **69**: 970–973.
4 Nakagawa K, *et al* (2009) First clinical cone-beam CT imaging during volumetric modulated arc therapy. Radiother Oncol **90**: 422–423.
5. Haga A, *et al* (2009) Quality assurance of volumetric modulated arc therapy using Elekta Synergy. Acta Oncol **48**: 1193–1197.
6. Qian J, *et al* (2010) Dose reconstruction for volumetric modulated arc therapy (VMAT) using cone-beam CT and dynamic log files. Phys Med Biol **55**: 3597–3610.
7. Wu C, *et al* (2002) Re-optimization in adaptive radiotherapy. Phys Med Biol **47**: 3181–3195.

Received on April 11, 2011
Accepted on May 6, 2011

Cone Beam Computed Tomography Data Acquisition during VMAT Delivery with Subsequent Respiratory Phase Sorting Based on Projection Image Cross-correlation*

Keiichi NAKAGAWA[1]*, Satoshi KIDA[1], Akihiro HAGA[1], Yoshitaka MASUTANI[1], Hideomi YAMASHITA[1], Toshikazu IMAE[1], Kenichiro TANAKA[1], Kuni OHTOMO[1], Yoshio IWAI[2] and Kiyoshi YODA[2]

4D CBCT/Respiratory phase/VMAT.

To The Editor

Localization and verification of a tumor position was conventionally performed prior to radiotherapy. The present authors, in the past a few years, proposed in-treatment verification of the tumor position by simultaneously acquiring cone beam computed tomography (CBCT) data using an on-board kilovolt imaging system. Dose delivery was either rotational conformal[1)] or volumetric modulated arc therapy (VMAT).[2,3)] The resulting three-dimensional (3D) volume image was appropriate for still organs such as prostate. For respiratory moving cases such as lung tumors, image blurring may be observed thereby reducing the accuracy of the tumor localization.

In the meantime, Sonke et al proposed four-dimensional (4D) CBCT for respiratory moving lung tumors[4)] assuming that the motion of the diaphragm correlates well with that of a lung tumor. The respiratory phase was calculated from frame-by-frame changes of projection images after enhancing diaphragm-like features on the cranio-caudal axis. Another group also published similar results later.[5)] Kavanagh et al proposed an alternative method for extracting a respiratory pattern from a set of projection images without relying on edge detection of the diaphragm position, where simple pixel value summation was employed followed by high pass filtering.[6)] Just recently, in ESTRO annual meeting, Sonke presented 4D CBCT during VMAT delivery by extending their previous 4D CBCT research for a lung tumor.[7)]

In this letter, we present our preliminary clinical 4D CBCT imaging during VMAT delivery using Elekta Synergy (Crawly, UK). As was described in our previous report,[1)] the current Synergy system does not allow simultaneous delivery of kV CBCT beams and MV rotational beams. Having known that kV portal imaging is available during MV rotational beam delivery, we developed in-house software for CBCT reconstruction by collecting all the kV portal images during gantry rotation. We have developed a new respiratory phase sorting algorithm based on image cross-correlation between adjacent two projection images. Image cross-correlation was previously used for registering a cone beam CT image with the planning CT image inside a specified region of interest while the former image was repeatedly shifted, and the patient treatment couch was displaced according to the shift vector for the highest correlation.[8)] Similarly cross-correlation between the adjacent two projection images was calculated while one of the images was shifted stepwise, and the shift vector giving the highest correlation was considered as the tumor displacement caused by breathing. In this algorithm edge detection is not employed and the image cross-correlation is an integral operation; in other words, it is less sensitive to image noise and diaphragm may not be required in the projection image.

Figures 1(a)–(e) show kV CBCT images of a lung tumor patient during VMAT delivery in four different respiratory phases: (a) reference 3D CBCT, (b) maximum exhalation, (c) mid inhalation, (d) maximum inhalation, and (e) mid exhalation. The cross lines indicate the isocenter. 2D image data were acquired during 2 minute, half gantry rotation with 652 projections. The number of bin was selected as four in this preliminary study to obtain a reasonable image contrast to noise ratio. The 4D image indicates that the tumor size is approximately 35 mm in the cranio-caudal direction, while the tumor size is detected as approximately 42 mm with 3D CBCT. In addition, it is found from 4D CBCT that the tumor movement amplitude is approximately 9 mm in the cranio-caudal direction.

In conclusion, we have shown that 4D CBCT data acqui-

*Corresponding author: Phone: +81-3-5800-9002,
Fax: +81-3-5800-8786,
E-mail: k-nak@fg7.so-net.ne.jp
[1]Department of Radiology, University of Tokyo Hospital, 7-3-1 Hongo Bunkyo-ku, Tokyo 113-8655, Japan; [2]Elekta, KK, 3-9-1 Shibaura, Minato-ku, Tokyo 108-0023, Japan.

Conflict of interest statement: Dr. Nakagawa receives research funding from Elekta.
doi:10.1269/jrr.10170

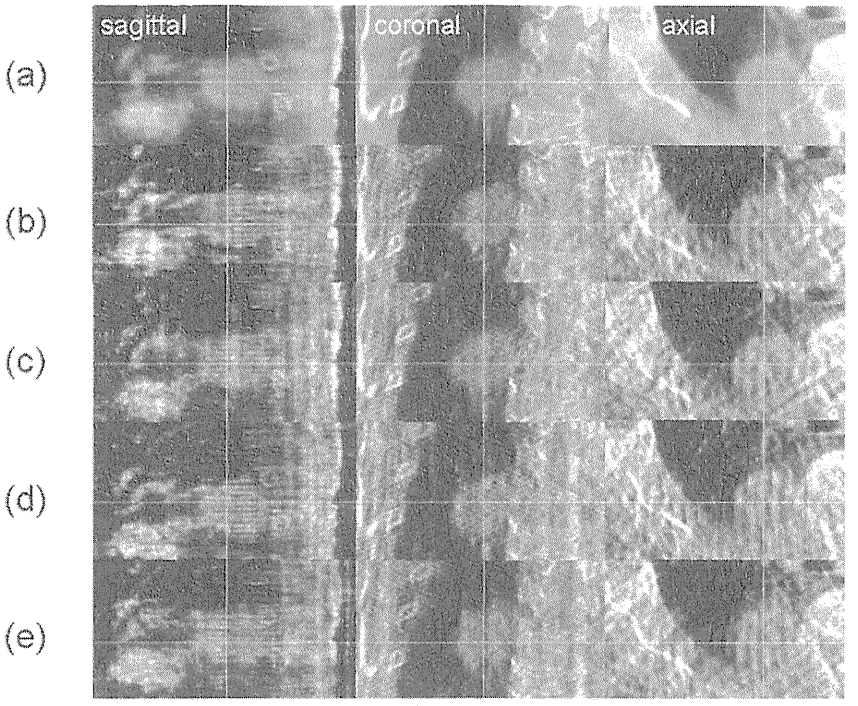

Fig. 1. kV 4D CBCT images of a lung tumor patient during VMAT delivery in four different respiratory phases: (a) reference 3D CBCT, (b) maximum exhalation, (c) mid inhalation, (d) maximum inhalation, and (e) mid exhalation. The cross lines indicate the isocenter. 2D image data were acquired during 2 minute, half gantry rotation with 652 projections. The 4D image indicates that the tumor size is approximately 35 mm in the cranio-caudal direction, while the tumor size is detected as approximately 42 mm with 3D CBCT. In addition, it is found from 4D CBCT that the tumor movement amplitude is approximately 9 mm in the cranio-caudal direction.

sition is feasible during VMAT delivery. Our respiratory phase sorting algorithm is different from previous ones and quantitative performance evaluation using large number of clinical cases is under consideration.

REFERENCES

1. Nakagawa K, *et al* (2007) Verification of in-treatment tumor position using kilovoltage cone-beam computed tomography: a preliminary study. Int J Radiat Oncol Biol Phys **69**: 970–973.
2. Nakagawa K, *et al* (2009) First clinical cone-beam CT imaging during volumetric modulated arc therapy. Radiother Oncol **90**: 422–423.
3. Nakagawa K, *et al* (2009) First report on prostate displacements immediately before and after treatment relative to the position during VMAT delivery. Acta Oncol **48**: 1206–1208.
4. Sonke JJ, *et al* (2005) Respiratory correlated cone beam CT. Med Phys **32**(4): 1176–1186.
5. Dietrich L, *et al* (2006) Linac-integrated 4D cone beam CT: first experimental results, Phys Med Biol **51**: 2939–2952
6. Kavanagh A, *et al* (2009) Obtaining breathing patterns from any sequential thoracic x-ray image set. Phys Med Biol **54**: 4879–4888
7. Sonke JJ, Remeijer P and van Herk M (2010) Four dimensional cone beam CT acquisition concurrent with VMAT delivery. Radiother Oncol **96**: **Suppl 1**, S75.
8. Sykes JR, *et al* (2005) A feasibility study for image guided radiotherapy using low dose, high speed, cone beam X-ray volumetric imaging. Radiother Oncol **77**: 45–52.

Received on December 4, 2010
Accepted on December 20, 2010

CI研究 32 (1) : 25-32, 2010

術中MRIシステムを用いた脳腫瘍手術

櫻田 香　竹村 直　久下 淳史
舟生 勇人　佐藤 慎哉　嘉山 孝正

A New Intraoperative MRI System in Brain Tumor Surgery

Kaori Sakurada, Sunao Takemura, Atsushi Kuge, Hayato Funiu,
Shinya Sato, and Takamasa Kayama

Department of Neurosurgery, Yamagata University Faculty of Medicine, Yamagata, Japan

(*Received August 27, 2009*)
(*Accepted February 26, 2010*)

Summary: *Background of Study*: Extensive surgical removal of brain tumors lengthens life expectancy. As dynamic changes, such as brain shift, can occur during surgical procedures, intraoperative MRI is an important tool for safe and maximum resection of tumors. In July 2008, new operating room equipped with an intraoperative high-field MRI (1.5T) system, neuronavigation, and fluorescence diagnosis system opened at the author's institution, Yamagata University Hospital.

Methods: Preoperatively, 3.0T MR studies, including morphological study, multivoxel MR spectroscopy, tractography and functional MRI, were performed. If the tumor was located in or near an eloquent area, we performed MEP (motor evoked potential)/SEP (sensory evoked potential) monitoring and/or awake surgery using cortical and subcortical stimulation. Intraoperative MRI was performed after total resection or to obtain updated information on brain positioning during the removal of deep-seated tumors.

Results: Using this new suite, we have safely treated various brain tumors, including gliomas, metastatic brain tumors, meningiomas, and pituitary adenomas. Gross total removal was achieved in over 70% of malignant tumors. Intraoperative MR images contributed to improving the tumor resection rate and overall results.

Key Words: Intraoperative MRI system, Brain surgery
使用機種: Achieva 3.0T (Philips) Signa 1.5T (GE), Neuronavigation (Brain Lab)

はじめに

fMRIやDiffusion Tensor Imagingなどの新しい画像診断法の進歩により脳腫瘍手術の計画をより綿密に立てることが可能となった．運動誘発電位や覚醒下手術などのモニタリング・マッピングを用いて最大限の安全な摘出を図ることが浸潤性に発育し病理学的には全摘出が不可能と考えられる悪性神経膠腫にとってもoptimalな治療であると認識されるようになってきている．現在ナビゲーションシステムや超音波診断装置の併用による摘出率の向上が試みられているが，brain shiftや超音波診断装置の解像度の問題もあり，術中に正確に残存腫瘍，摘出率を把握することは困難である．2008年7月，当科で1.5テスラ術中MRIシステム（1.5T MRI (GE)，neuronavigation (Brain LAB)，術中蛍光診断・術中血管撮影機能FL400，FL800（KARL-STORZ）搭載手術顕微鏡（Leica），MRI・CT対応operation table (MAQUET)）を導入したので，新インテリジェント手術システムとその使用経験につき報告する．

山形大学医学部 脳神経外科【連絡先：〒990-9585 山形県山形市飯田西 2-2-2】

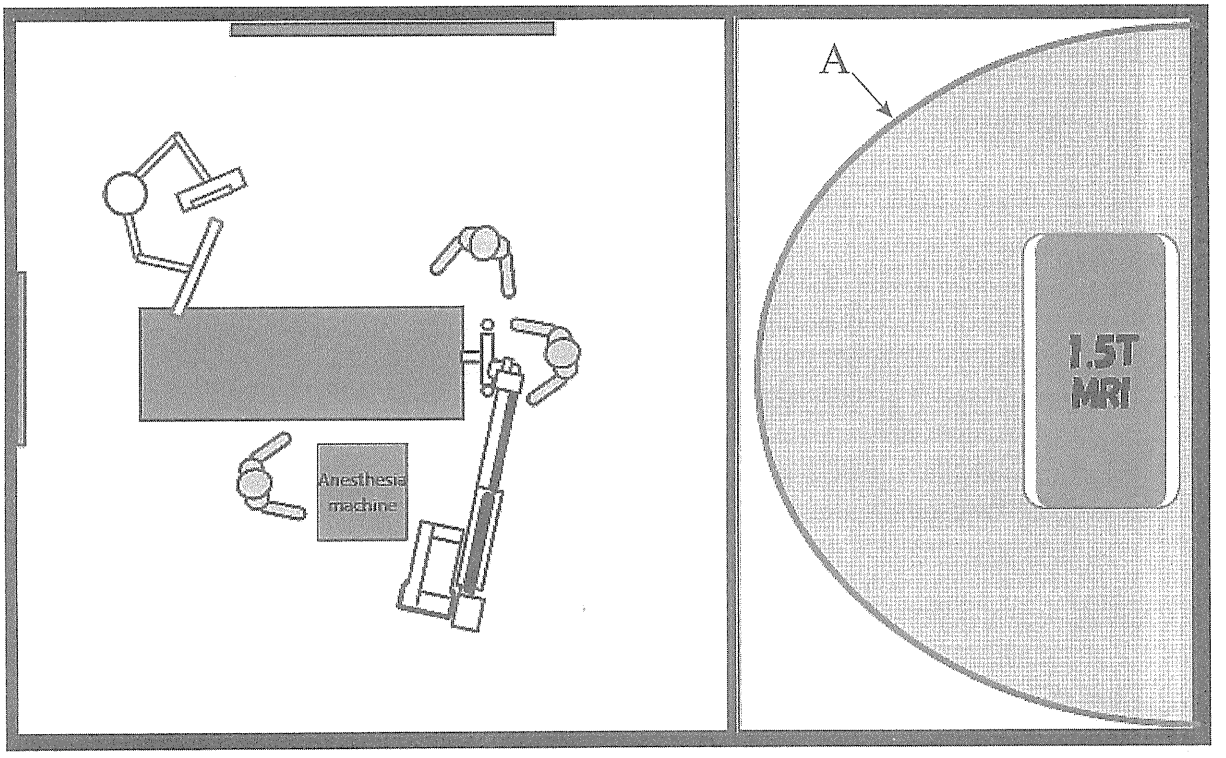

Fig. 1 Scheme of the new operation room. *line A* is 5-gauss line.

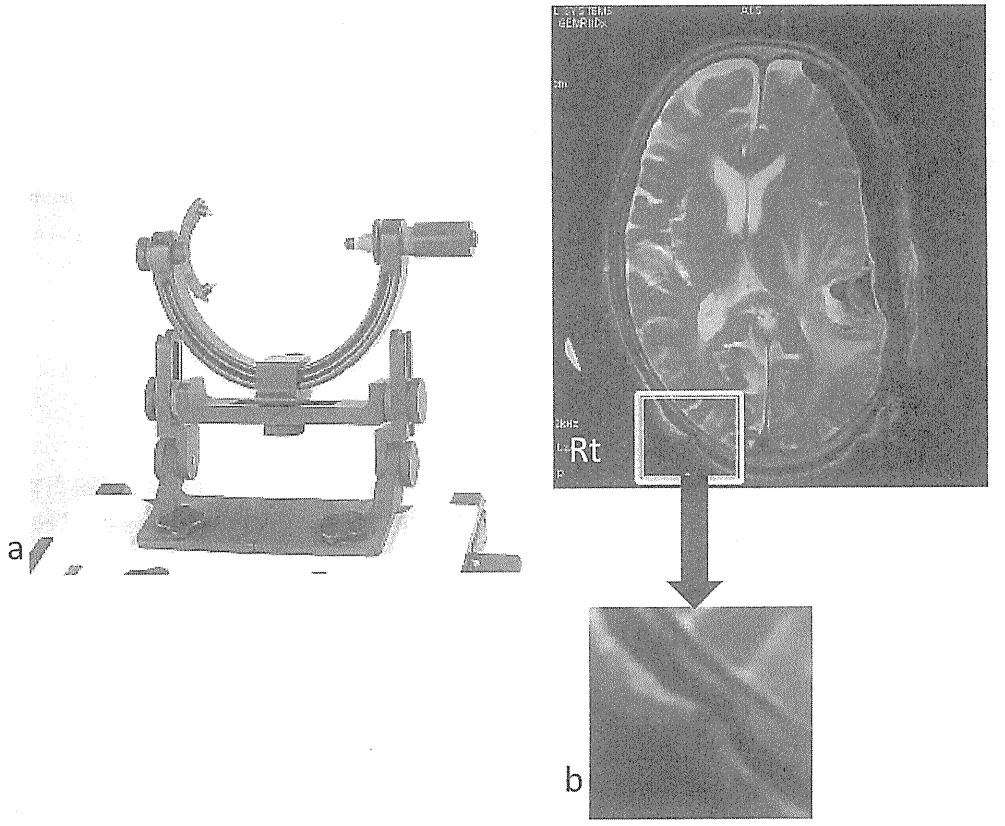

Fig. 2 **a**: Mayfield head clamp. **b**: MR image shows no artifact caused by head pin.

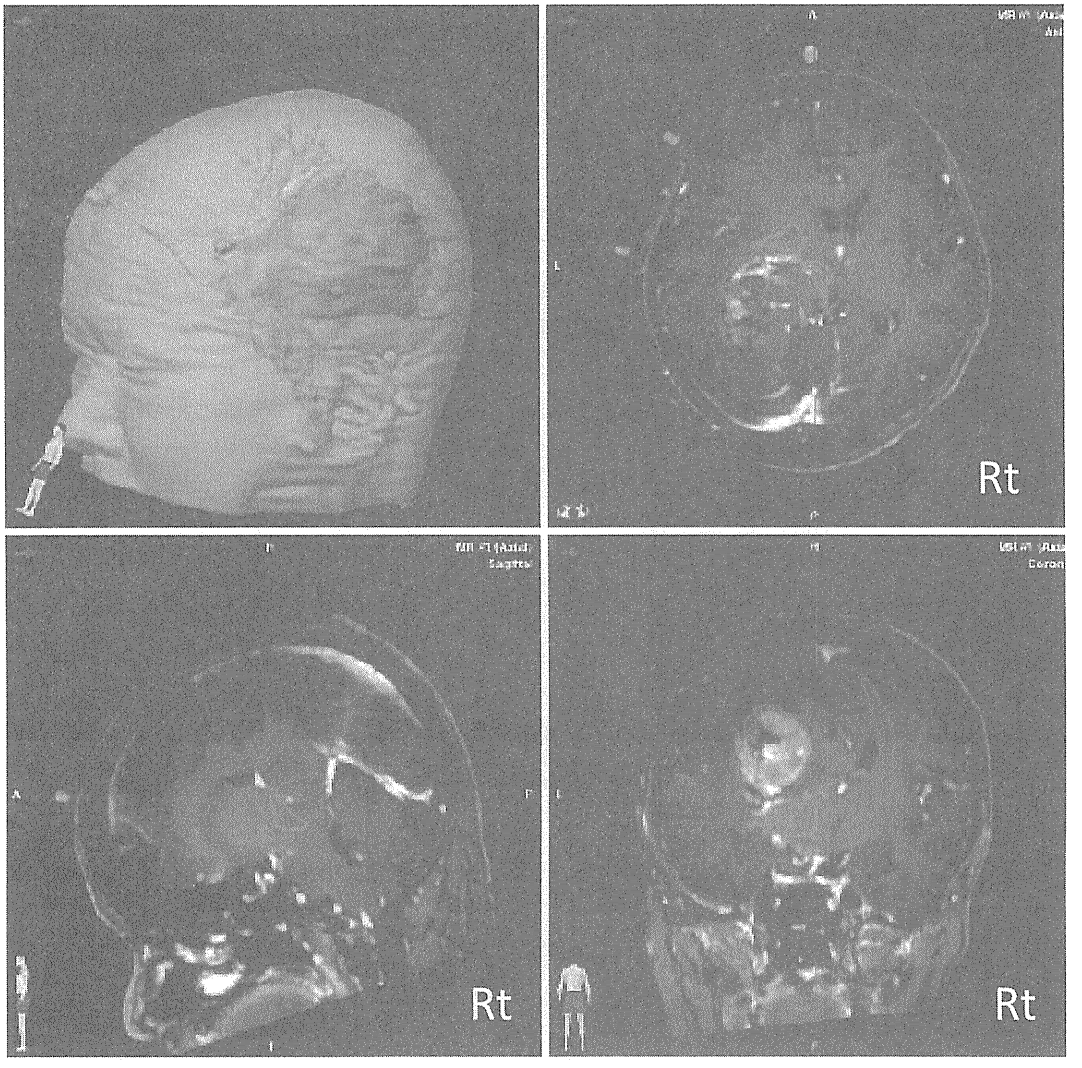

Fig. 3 T1-weighted images are displayed in axial, coronal and sagittal planes, as well as a 3-D rendering, depicting the three objects: tumor (*red*), fMRI (*yellow*), and pyramidal tract (*green*).

新手術室システム

当院に導入された術中MRIシステムは，いわゆるtwin-operating theaterといわれる形で，手術室とMRI検査室が2つの部屋に分かれている(**Fig. 1**)．このシステムの利点は，既存の手術器具をそのまま使用し従来とほぼ同じ環境で手術操作が可能，また手術患者の撮影を行っていないときには他の患者の検査が施行できるという経済的なメリットがある．しかしながら，MRIおよび手術室が一体となったシステムに比べ患者の移動距離が長くなるという不利な点もある．幸い当院では，麻酔科，その他co-medicalの理解と協力によりこれまで問題なく安全かつ迅速な患者移動および検査が行えている．MRIは1.5T(GE)の高磁場MRIが導入され，高磁場MRIによる精細な画像とMRA，MRS，tractographyなどの撮影が可能である．Neuronavigation（Brain Lab)は，院内の画像サーバーと術中MRIの両方から画像を取り込むことができ，術中画像は数分でナビゲーションシステムに転送され，再レジストレーションなく患者がMRI終了し手術再開までにup-dateが完了する．2009年4月より，術前に3.0T MRIで撮影したデータを用いて，術中fMRI，tractographyを合成する機能も追加となった．頭部固定は，カーボンファイバー製のメイフィールド3点固定装置でCT，angiography，MRIに対応している．ピンはサファイヤ製でMRIでもアーチファクトがほとんど生じない(**Fig. 2**)．術中蛍光診断システムとしては，KARL-STORZのFL400, FL800が，顕微鏡に搭載され，5-アミノレブリン酸による腫瘍蛍光診断と，ICGを用いた蛍光血管撮影が可能である．5-ALAの蛍光診断には，蛍光診断装置（M&M VLD-1)を用いてスペクトル解析も行い，肉眼では認識困難

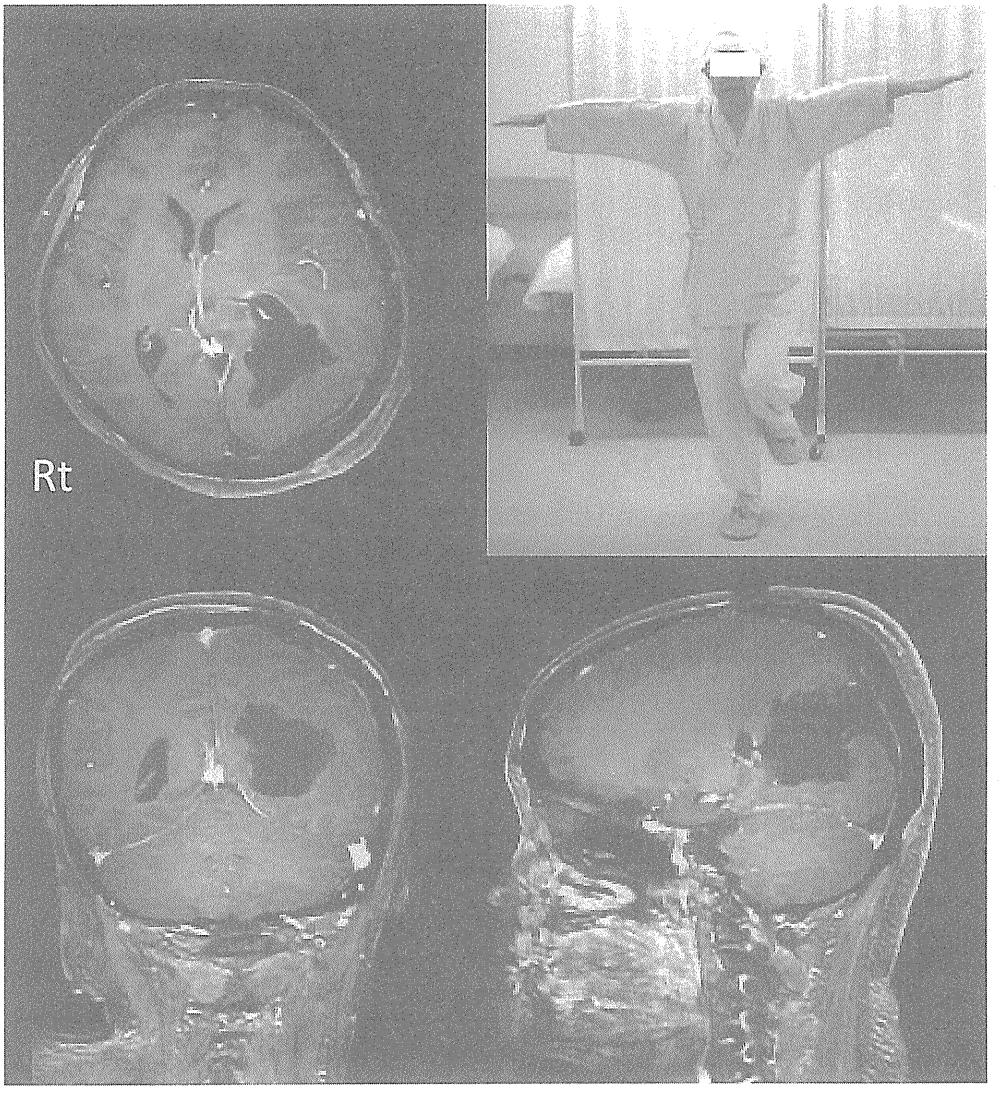

Fig. 4　Post-operative images show gross total removal of the tumor. Rt. motor weakness was improved after the operation.

な淡い蛍光を検出し腫瘍摘出度を向上させ局所再発率の低下を期待している.

対象と方法

2008年7月から2009年2月までに，32例の脳神経外科手術を施行した．内訳は，神経膠腫 14例，転移性脳腫瘍 3例，下垂体腺腫 7例，髄膜腫 3例，未破裂脳動脈瘤 3例，側頭葉てんかん（選択的海馬摘出術）2例，AVM 1例である．術中 MRI システムの最も良い適応は脳実質内腫瘍であるが，当科では腫瘍性病変以外の手術にも積極的に本システムを活用している．MRI 検査は，DWI，T1, T2, FLAIR，造影3方向と脳動脈瘤・AVM では MRA も追加し，摘出率，虚血・出血病変などの有無の評価を行った.

症例呈示

症例 1：54歳女性．Lt. parietal glioblastoma

右半身脱力と視野障害を主訴に来院した．MRI にて Lt. parieto-occipital に径 5cm の腫瘍を認めた．Tractography では，錐体路は腫瘍により前方に圧排されていた.（**Fig. 3**）開頭脳腫瘍摘出術を施行した．ナビゲーションに fMRI および tractography データを重ね，更に MEP による運動モニタリングを併用し，腫瘍を全摘出した．術中 MEP モニタリングで変化なく，MRI にて造影域の全摘出を確認して手術を終了した．術後，右片麻痺は消失した（**Fig. 4**）.

結　果

神経膠腫および転移性脳腫瘍 17例の手術摘出率を示す.

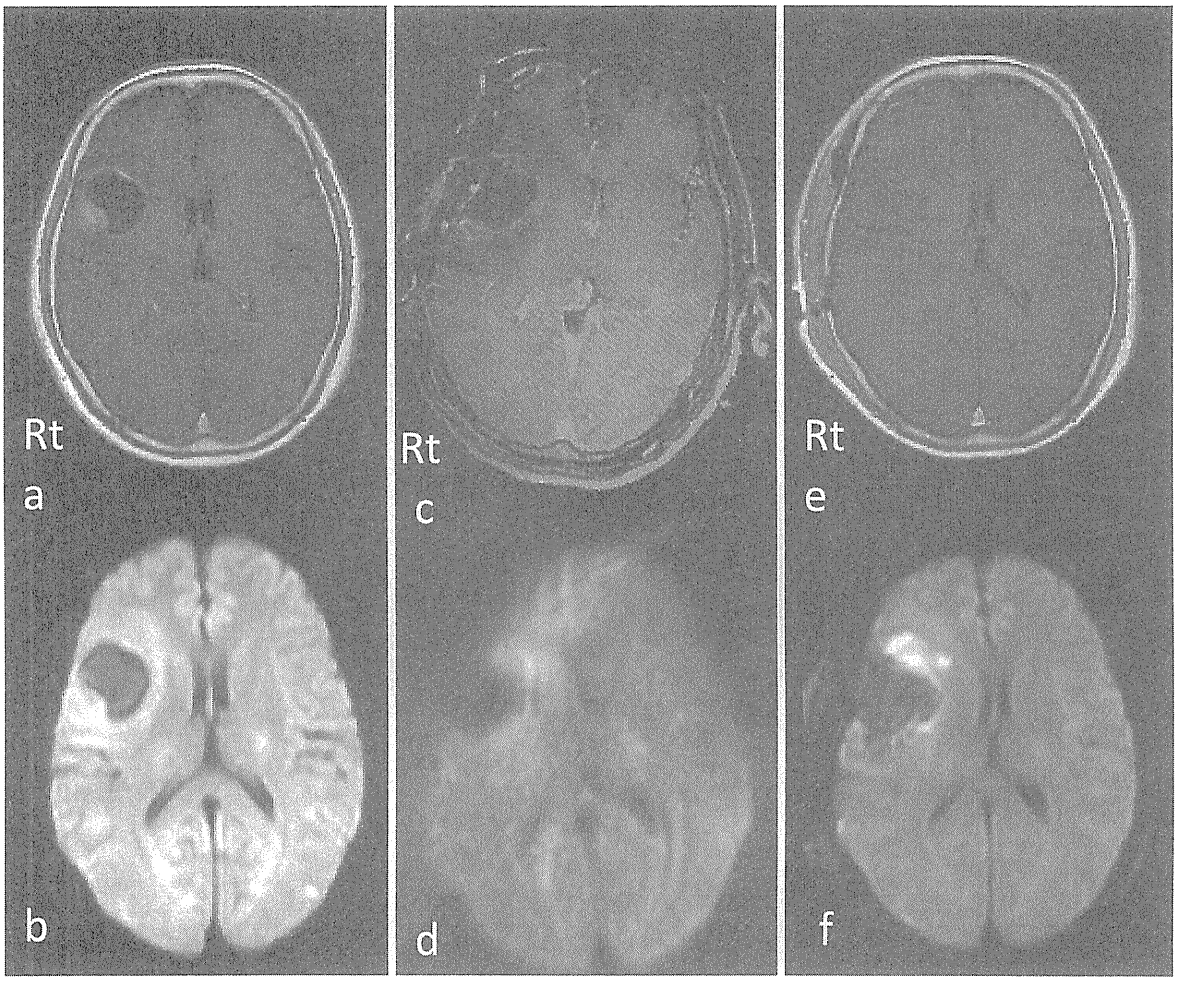

Fig. 5 Post-operative DW image revealed high signal area adjacent to the resection cavity (**e, f**). Intraoperative MR images do not show the abnormal intensity area (**c, d**). Preoperative MR images (**a, b**).

術中MRIにてGross total resection（GTR）は13例（76.5%）で得られた．術中MRI後に追加切除を加えた例は2例であった．脳梁を介して対側まで病変が及んでいた左前頭葉GBMと再発小脳GBMであり，摘出率の向上は得られたが，GTRまでは及ばなかった．術者がGTRと判断したにもかかわらず残存病変を認めた例はなかった．術中MRIの拡散強調画像にて，虚血病変を認めた症例はなかったが，術後MRIで腫瘍切断端にDWI高信号を認めた例が数例みられたことから，術中では手術操作から撮影までの時間が短く検出が困難であったと考えられた(**Fig. 5**)．出血に関しては，術翌日のCTにて摘出腔内に少量の出血を認めた鞍上部Gliomaにおいて，術中DWIにて同部位が高信号を呈していたことから，出血から撮像までの時間経過が影響するが，DWIにて術中の出血を検出できる可能性が示唆された(**Fig. 6**)．感染などの術中MRIに関連する合併症はこれまで認めていない．

考　察

術中MRIは，1993年ボストンのBrigham and Women's hospitalに世界に初めて導入され，その後世界各地で種々のシステムが開発され徐々に普及してきている[1)2)3)5)6)7)8)12)13)]．世界初のシステムは，0.3Tの低磁場MRIでコイルを縦に配置したDouble doughnut型といわれるもので，手術はコイルの間で行われ専用の手術器具を要するシステムである．日本でも同一システムが2000年に滋賀医科大学に日本初の術中MRIシステムとして導入された．同年，東京女子医科大学に導入されたシステムは，同じく低磁場MRIであるが，コイルを水平に配置し，手術を5ガウスラインより外側で行うことにより既存の手術機器がそのまま使用できるシステムである．また東京女子医科大学では，術中MRIだけではなく，ナビゲーションシステムおよび手術室情報管理システムを構築し，インテリジェント手術室という新たな概念を提唱した[15)16)]．2008年7月に稼働開始した当院

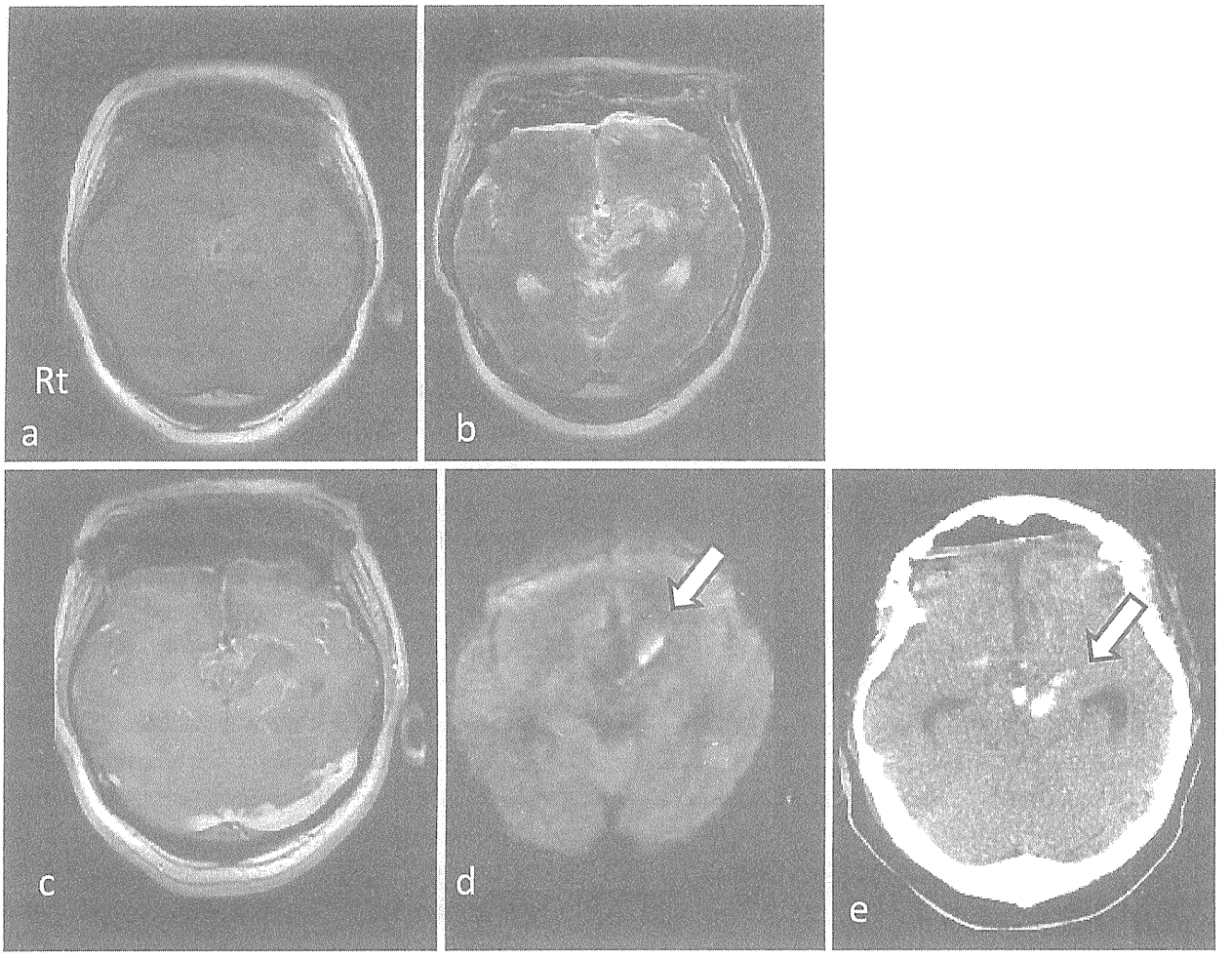

Fig. 6　Intraoperative MR images (**a**: T1-weighted, **b**: T2-weighted, **c**: T1 with Gadolinium, **d**: DWI). Intraoperative DW image shows intra-tumoral hemorrhage (**d**: *open arrow*). Post-operative CT shows the intra-tumoral hemorrhage (**e**: *open arrow*).

の新術中 MRI システムは国内 8 番目のものであり，高磁場 MRI システムとしては，2006 年の名古屋セントラル病院，東海大学についで日本で 3 番目となるものである[11)12)]．

術中 MRI システムが脳神経外科手術にもたらす利点としては，brain shift を up-date し手術中の navigation の精度を上げ安全に腫瘍摘出率を向上させうるということ，また術野内・外の術中の予想外のイベントを察知できることがあげられる[14)17)18)20)]．MRI による摘出率の判定を行うことにより，浸潤性に発育する glioma においても，手術摘出率が予後因子の 1 つであることが広く認められるようになり，術中 MRI システムを用いた摘出率向上は患者の予後向上に寄与するものと期待される[10)21)]．実際に 2005 年 Claus らは，術中 MRI を用いて腫瘍摘出を行った場合に glioma 患者の予後改善がみられたことを報告している[4)]．

術中 MRI は，すべての脳腫瘍手術に用いることが理想であるが，術中 MRI の必要度・貢献度は当然症例毎に異なる．また MRI のボアサイズ（患者撮影部位直径）による体位・頭位の制限もあり，現時点では全例に用いることは困難である．MRI のボアサイズ，コイル等の改良，頭部固定具，手術台の改良が必要である．

これまで悪性神経膠腫の摘出率の判定には，術後 48 時間以内の造影 T1 強調画像が用いられ，この判定に基づいた摘出率と予後との関係が検討されてきた．術中 MRI の自験例では，術中の trauma によっても造影剤漏出がみられることがあり，術中 MRI による残存腫瘍の判定に際して注意を要するものと考えている[9)]．特に，腫瘍が正常脳に覆われて，正常脳が庇になっている部位は顕微鏡の死角となりやすく腫瘍残存しやすい．また庇となっている正常脳を脳ベラなどで移動することにより trauma が生じやすくこの部位から造影剤が漏出する可能性がある．腫瘍切除端の造影域が残存腫瘍であるのか，挫滅された脳なのか判断に注意を要する．術中画像のみにとらわれることなく，術前画像で in-

ternal control となる脳溝・動静脈などと腫瘍境界との関係をしっかり把握することが，術中MRI・ナビゲーションシステムを用いた手術でも重要である．

極めて浸潤能の高い悪性神経膠腫に対して，病理組織学的な全摘出を完遂することは難しい．しかし，治療後の再発のほとんどが局所再発であることから[19]，MRI造影病変の辺縁に存在する腫瘍細胞が高密度に浸潤していると考えられる部位をより多く摘出することが重要であると考えられる．MRI造影病変は色調や硬さなどによりある程度鑑別できるが，造影域辺縁の浸潤部位の最大限の摘出を目指す場合，術中MRIおよび術中蛍光診断の貢献度は大きいと考える．術中MRIシステムによる摘出率，治療成績の変化について検討するとともに，放射線・化学療法をはじめとする後療法の改良・開拓も今後の重要な課題である．

結　語

2008年7月，当科で1.5テスラ術中MRIシステム（1.5T MRI（GE），neuronavigation（Brain LAB），術中蛍光診断・術中血管撮影機能FL400, FL800（KARL-STORZ）搭載手術顕微鏡（Leica），MRI・CT対応 operation table（MAQUET））を導入した．本新システムを使用して安全に脳神経外科手術を施行し，悪性脳腫瘍の70％以上でGross total removalがなされた．今後，他の脳神経外科手術への応用と悪性脳腫瘍の予後改善に対する本システムの有用性を検討したいと考えている．

文　献

1) Albayrak B, Samdani AF, and Black P: Intra-operative magnetic resonance imaging in neurosurgery. Acta Neurochir **146**: 543-557, 2004
2) Black PM, Alexander E 3rd, Martin C, et al: Craniotomy for tumor treatment in an intraoperative magnetic resonance imaging unit. Neurosurgery **45**: 423-430, 1999
3) Black PM, Moriarty T, Alexander E 3rd, et al: Development and implementation of intraoperative magnetic resonance imaging and its neurosurgical applications. Neurosurgery **41**: 831-845, 1997
4) Claus EB, Horlacher A, Hsu L, et al: Survival rates in patients with low-grade glioma after intraoperative magnetic resonance image guide. Cancer **103**: 1227-1233, 2005
5) Fahlbusch R, Ganslandt O, Buchfelder M, et al: Intraoperative magnetic resonance imaging during transsphenoidal surgery. J Neurosurg **95**: 381-390, 2001
6) Hall WA, Liu H, Maxwell RE, et al: Infuluence of 1.5-Tesla intraoperative MR imaging on surgical decision making. Acta Neurochir **85** (suppl): 29-37, 2002
7) Hall WA, and Truwit CL: Intraoperative MR-Guided Neurosurgery. J Magn Reson Imaging **27**: 368-375, 2008
8) Hushek SG, Martin AJ, Steckner M, et al: MR systems for MRI-Guided Interventions. J Magn Reson Imaging **27**: 253-266, 2008
9) Knauth M, Aras N, Rainer C, et al: Surgically induced intracranial contrast enhancement: potential source of diagnostic error in intraoperative MR imaging. AJNR **20**: 1547-1553, 1999
10) Lacroix M, Abi-Said D, Fourney DR, et al: A multivariate analysis of 416 patients with glioblastoma multiforme:prognosis, extent of resection, and survival. J Neurosurg **95**: 190-198, 2001
11) Maesawa S, Fujii M, Nakahara N, et al: Clinical indications for high-field 1.5T intraoperative magnetic resonance imaging and Neuro-navigation for neurosurgical procedures. Neurol Med Chir (Tokyo) **49**: 340-350, 2009
12) 松前光紀，厚見秀樹：画像誘導治療．脳神経外科 **35**: 329-342, 2007
13) Matsumae M, Koizumi J, Fukuyama H, et al: World's first magnetic resonance imaging/x-ray/operating room suite: a significant milestone in the improvement of neurosurgical diagnosis and treatment. J Neurosurg **107**: 266-273, 2007
14) McClain CD, Soriano SG, Goumnerova LC, et al: Detection of unanticipated intracranial hemorrhage during intraoperative magnetic resonance image-guided neurosurgery. J Neurosurg **106** (**5** Suppl Pediatrics): 398-400, 2007
15) 村垣善浩：術中MRI. NS Now **5**: 104-111, 2008
16) Muragaki Y, Iseki H, Maruyama T, et al: Usefulness of intraoperative magnetic resonance imaging for glioma surgery. Acta Neurochir Suppl **98**: 67-75, 2006
17) Nimsky C, Ganslandt O, Cerny S, et al: Quantification of, visualization of, and compensation for brain shift using intraoperative magnetic resonance imaging. Neurosurgery **47**: 1070-1080, 2000
18) Nimsky C, Ganslandt O, Hastreiter P, et al: Preoperative and intraoperative diffusion tensor imaging-based fiber tracking in glioma surgery. Nueurosurgery **56**: 130-138, 2005
19) Oppitz U, Maessen D, Zunterer H, et al: 3D-recurrence-pattern of glioblastomas after CT-planned postoperative irradiation. Radiotherapy and Oncology **53**: 53-57, 1999
20) Ozawa N, Muragaki Y, Nakamura R, et al: Shift of the Pyramidal tract during resection of the intraaxial brain tumors estimated by intraoperative diffusion-weighted imaging. Neurol Med Chir **49**: 51-56, 2009

21) The Comittee of the Brain Tumor Registry of Japan: Report of Brain Tumor Registry Japan (1984-2000), 12th ed. Neurol Med Chir (Tokyo) **49**: 1-101, 2009

Comments

著者らは，本論文にて高磁場 MRI 等を備えた統合型手術室を用いた脳腫瘍治療について，その有用性について記載した．手術手技，および手術支援装置の進歩にともなって，浸潤性の高い腫瘍である glioma においても，手術摘出の重要性の指摘がされてきている．より安全にかつ摘出度をあげるために，著者らは統合型手術室において，種々の工夫を行っている．本論文は将来の手術室の方向性を示し，またこのような手術室をあらたに設置しつつある者にとって，参考となる記載に富んだ論文である．

藤巻 高光（埼玉医科大学病院 脳神経外科）

術中 MRI 等を組み合わせたインテリジェント手術システムについての報告である．摘出度を上げると共に術後の神経症状の悪化を防ぎ，手術成績を向上するために様々な努力がなされて来たが，その最先端が結集されている．術中 MRI は腫瘍の摘出度を知る以外にも合併症の有無についての check もできる点で有用であるが，そのコストと移動や撮影に時間を要することが問題である．High-grade glioma の多くでは蛍光システムで代用出来るが，low-grade glioma などの造影を受けない病変での有用性は現在のところ他に変わるものはないだろう．多くの病院ではこのようにすべてをそろえることは不可能であり，どの機器がどのような手術の時に有用なのかを今後検証して行って欲しい．

中洲 敏（草津総合病院 脳腫瘍治療科）